Prediction of Static Aerodynamic Characteristics of Air Cushion Vehicles through 180° of Yaw

WALTER ZEITFUSS Jr.* and EUGENE N. BROOKS Jr.*
Naval Ship Research and Development Center, Bethesda, Md.

A method for predicting the static, directional aerodynamic characteristics of varying air cushion vehicle geometries to yaw angles of 180° and speeds to 120 knots has been developed and programed for use on the CDC 6700 digital computer. The predictions are based on linear and nonlinear variations from the aerodynamic characteristics of a basic configuration. The drag, side force, and yawing moment investigated include only external forces and moments and do not include the forces and moments produced by the cushion itself. Predictions are compared with experimental data to demonstrate the accuracy of the method. It is felt this prediction represents a valuable advance in the state of the art of ACV aerodynamics. The lack of a similar program to date has necessitated expensive and time consuming wind-tunnel testing of individual ACV configurations.

Nomenclature†

AA, BA	= aft, bow angle to bottom plane (Fig. 1)
ACV	= air cushion vehicle
b	= vehicle maximum width ft (Fig. 1)
C_D	= drag coefficient = D/qlb, wind axis
C_N	= yawing moment coefficient = N/ql^2b, wind axis
C_Y	= side force coefficient = Y/qlb, wind axis
D	= drag force, lb
H	= vehicle height not including superstructure (Fig. 1), ft
h_a	= aft height of aft angle (Fig. 1) ft
h_f	= front height of bow angle (Fig. 1) ft
l	= vehicle maximum length (Fig. 1) ft
l_{FD}	= length from nose to superstructure (Fig. 1) ft
l_s	= length of superstructure (Fig. 1) ft
N	= yawing moment, ft-lb
p_c	= cushion pressure, psf
q	= freestream dynamic pressure = $\frac{1}{2}\rho V^2$, psf
R_B, R_A	= bow, aft planform radius (Fig. 1), ft
r	= edge radius (Figs. 1 and 2), ft
V	= freestream velocity, fps
x	= bow or aft side contour length (Fig. 1) ft
X_0, X_1, X_2	= coefficients of 1, β, β^2 of second-order variation
XCP	= length from center of pressure (at $\beta = 90°$) to aft end, ft
XCG	= length from moment reference point or center of gravity to aft end, ft
Y	= side force, lb
y	= bow or aft side contour height (Fig. 1) ft
$\Delta C_{ij}(\beta)$	= change in C_D, C_Y, $C_N (i = D, Y, N)$ due to jth geometry parameter (j = ASC, BP, AA, ...) from C_D, C_Y, C_N for basic vehicle as function of β
$\partial C_i/\partial j$	= slope of curve for C_D, C_Y, C_N vs jth geometry parameter
β	= yaw angle, deg
ρ	= free stream density, slugs/ft³

Subscripts

BASIC	= pertaining to basic vehicle (Fig. 4)
K	= pertaining to a particular configuration
0°–45°	= in the range of $0° \leqslant \beta \leqslant 45°$
135°–180°	= in the range $135° \leqslant \beta \leqslant 180°$

Presented as Paper 71-907 at the AIAA Guidance, Control and Flight Mechanics Conference, Hempstead, New York, August 16–18, 1971; submitted September, 1, 1971; revision received December 27, 1971.

Index category: Ground (or Water-Surface) Effect Machines.

* Aerospace Engineer.

† Nondimensionalized geometric parameters are defined by Table 1 and Fig. 2.

Introduction

INITIAL work by the Navy on an Arctic Air Cushion Vehicle (ACV) indicated a need to develop the capability of predicting the external aerodynamic characteristics of general ACV shapes in ground effect to yaw angles of 180° and to speeds of 120 knots. Because the ACV has little or no ground contact, it has the advantages of being terrain independent and of requiring little propulsive force to overcome ground contact friction. However, this same lack of ground contact makes the vehicle solely dependent upon aerodynamic forces for its maneuvering and control characteristics. The performance and handling characteristics of the ACV are heavily dependent on external aerodynamics, particularly at high speeds and under high wind conditions expected in Arctic operations. A literature search revealed that aerodynamic prediction methods for ACVs are virtually nonexistent. Aerodynamics work in the past has depended on wind-tunnel tests for each vehicle configuration. Because the primary maneuvering of an Arctic ACV will be done in the yaw plane, the present work was undertaken to develop a method for predicting the directional aerodynamic characteristics to 180° of yaw for varying speeds. Yaw angles to 180° must be investigated because large angles of yaw are frequently encountered, either due to vehicle maneuvers such as pirouettes or due to high-speed trailing winds combined with low vehicle ground speeds.

Vehicle Geometry Parametrization

In order to correlate existing tunnel data on various ACV shapes, we have characterized the vehicle geometry by the dimensions shown in Fig. 1 and have defined nondimensionalized geometric parameters plus two angles as listed in

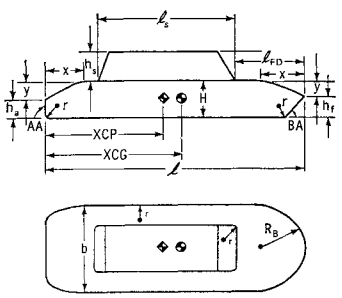

Fig. 1 Vehicle geometry and dimensions.

Table 1 Order of C_D, C_Y, C_N variations for geometry parameters

Parameter	Symbol	Order of Variation		
		C_D	C_Y	C_N
Bow side contour $= (x + y)/H$	BSC	1	1	1
Bow planform $= R_B/(b/2)$	BP	1	1	2, 1[a]
Bow angle, deg	BA	2	2	2
Aft side contour $= (x + y)/H$	ASC	1	1	1
Aft planform $= R_A/(b/2)$	AP	1	1	1
Aft angle, deg	AA	2	2	2
Aft height ratio $= h_a/H$	AHR	1	1	1
Forward height ratio $= h_f/H$	FHR	1	1	1
Superstructure height $= h_s/H$	SSHT	1	1	2
Superstructure length $= l_s/l$	SSL	1	1	1
Superstructure foredeck $= l_{FD}/l$	SSFD	2	2	2
Length/beam ratio $= l/b$	XLB	2	2	2
Edge radius $= r/l$	ER	1	2	2

[a] Second order for $0.824 < BP < 2.5$, first order for $BP < 0.824$.

Table 1 and illustrated in Fig. 2. These parameters have first-order (linear) or second-order effects on the drag, side force, and yawing moment coefficients as indicated in Table 1. Of course there are other geometry variations, but the ones defined here and used in this method are believed to be sufficient to characterize a large number of vehicles. All forces and moments presented in this paper are in yaw plane with the wind axis system shown in Fig. 3.

Prediction Method

Because of the lack of sophisticated fluid flow analysis methods for the rather irregular three-dimensional shapes by which ACV's are usually characterized, it was decided to correlate existing wind-tunnel data on ACV shapes and empirically fit the variations of drag, side force, and yawing moment due to variations in the described geometry parameters. Thus, a basic configuration shown in Fig. 4 was chosen, and its geometric parameters were defined as "basic". The effects of a change in any one of these parameters on C_D, C_Y, and C_N were then determined, as discussed below, and these effects were then added to the C_D, C_Y, and C_N of the basic configuration; i.e.,

$$C_i(\beta) = C_{i_{\text{BASIC}}}(\beta) + \sum_j \Delta C_{ij}(\beta) \; (i = D, Y, N) \qquad (1)$$

$$C_D(\beta) = C_{D_{\text{BASIC}}}(\beta) + \Delta C_{D_{BSC}}(\beta) + \Delta C_{D_{BP}}(\beta) + \Delta C_{D_{BA}}(\beta) + \cdots \qquad (2)$$

where $\cdots$ represents the effects of other geometrical effects; $C_{i_{\text{BASIC}}}(\beta)$ is the variation of the force component

$$(i = D, Y, \text{or } N)$$

of the basic vehicle with yaw angle and $\Delta C_{ij}(\beta)$ is the change in that component due to the jth geometrical change.

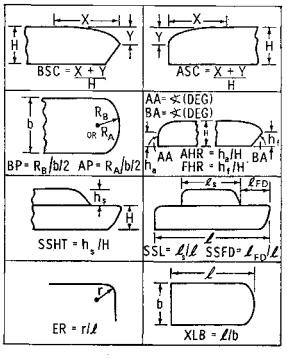

Fig. 2 Geometrical parameters.

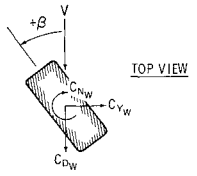

Fig. 3 Forces in the yaw (horizontal) plane.

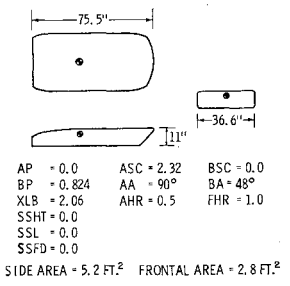

Fig. 4 Basic configuration and its parameters.

The aerodynamic characteristics of the basic vehicle are shown in Fig. 5. These "basic curves" are eighth-order curve fits of data from Refs. 1 and 2.

Since the methods of predicting the various geometrical effects are similar, only a few will be discussed in detail. It should be made clear that each $\Delta C_{ij}(\beta)$ only includes the *difference* from the ith curve in Fig. 5 due to that particular (jth) geometry deviation from the basic vehicle. For example, $\Delta C_{D_{BSC}}(\beta)$ is the change in drag coefficient (as a function of β) due to changes in the bow side contour *BSC* from that of the basic vehicle.

Drag coefficient data for $BSC = 0$, 1.362, and 2.42 from Ref. 1 are plotted in Fig. 6. Since the drag coefficient varies approximately linearly with *BSC* for each β, a straight line was assumed through each set of three points as indicated in the figure. The slopes of these straight lines were then plotted vs β as shown in Fig. 7, and a fourth-order curve fit was

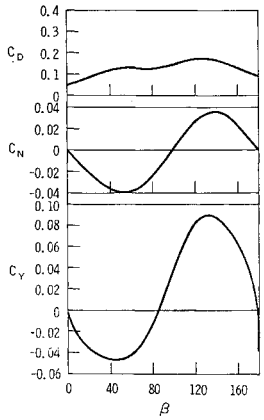

Fig. 5 Aerodynamic characteristics of the basic configuration.

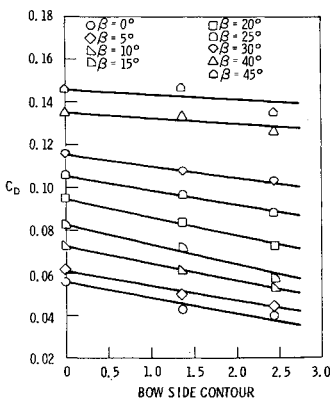

Fig. 6 Change in C_D due to changes in bow side contour.

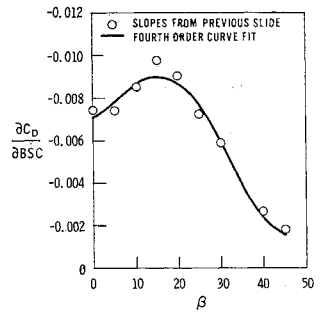

Fig. 7 Slopes of drag coefficient bow side contour vs β.

obtained for use in the program. Then for any new configuration of interest,

$$\Delta C_{D_{BSC}}(\beta) = (\partial(C_D)/\partial\, BSC)(\beta) \cdot (BSC - BSC_{\text{BASIC}}) \quad (3)$$

and since $BSC_{\text{BASIC}} = 0$

$$\Delta C_{D_{BSC}}(\beta) = (\partial(C_D)/\partial\, BSC)(\beta) \cdot BSC \quad (4)$$

The variation in drag due to bow planform $\Delta C_{D_{BP}}(\beta)$ was also found to be approximately linear; however, BP_{BASIC} is 0.824; therefore, the following equation results:

$$\Delta C_{D_{BP}}(\beta) = \frac{\partial(C_D)}{\partial\, BP}(\beta) \cdot (BP - 0.824) \quad (5)$$

The variation in drag due to bow angle $\Delta C_{D_{BA}}(\beta)$ was not linear, but approximately second-order as shown in Fig. 8. Second-order curve fits were made of this variation in the form:

$$C_D = X_0 + X_1(BA) + X_2(BA)^2 \quad (6)$$

where X_0, X_1, and X_2 are coefficients which, for this parameter, are not functions of β, but for other parameters these coefficients of second-order variations may vary with β, so that the general forms of the equations to be used are:

$$(C_{D_J})_{\text{BASIC}} = X_0(\beta) + X_1(\beta) \cdot j_{\text{BASIC}} + X_2(\beta) \cdot (j_{\text{BASIC}})^2 \quad (7)$$

$$(C_{D_J})_K = X_0(\beta) + X_1(\beta) \cdot j + X_2(\beta) \cdot (j)^2 \quad (8)$$

$$\Delta C_{D_J} = (C_{D_J})_{\text{BASIC}} - (C_{D_J})_K \quad (9)$$

The remaining variations in ΔC_D($\Delta C_{D_{ASC}}$, $\Delta C_{D_{AP}}$, $\Delta C_{D_{AA}}$, $\Delta C_{D_{SSHT}}$, $\Delta C_{D_{SSL}}$, $\Delta C_{D_{SSFD}}$, $\Delta C_{D_{XLB}}$, and $\Delta C_{D_{ER}}$) are handled in a similar manner to the preceding cases, i.e., by Eq. (3) for a first-order variation or by Eqs. (7–9) for a second-order variation. The order of variation with each geometry parameter is listed in Table 1.

These variations in some cases were deduced by the authors from a limited amount of data available. It will be seen later, however, that they yield very good predictions of the characteristics of a number of vehicles. When more data become available, they can be revised if necessary.

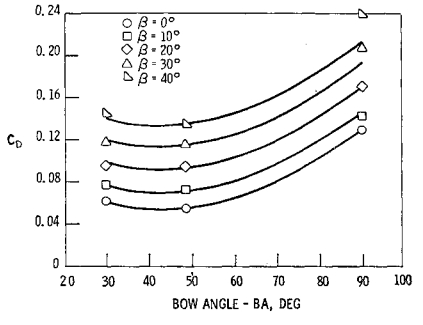

Fig. 8 Changes in C_D due to changes in bow angle.

Since data from Ref. 1 were available only to 45° of yaw, the following method was used to predict the $\Delta C_{D_J}(\beta)$ at higher angles. For $135° \leq \beta \leq 180°$, the $\Delta C_{D_J}(\beta)$ variations obtained for 0 to 45° were added to the $C_{D_{\text{BASIC}}}$. However, since in general the geometry characteristics of the aft end of the configuration under consideration are different than those for the bow, the aft geometry parameters were used, and the aft and bow parameters were interchanged where necessary. Thus, *BSC* and *ASC* were interchanged, *BP* and *AP* were interchanged, etc. For example, Eq. (3) for the aft end becomes:

$$[\Delta C_{D_{BSC}}(\beta)]_{135°-180°} = \frac{\partial(C_D)}{\partial\, BSC}(\beta) \cdot (ASC - 2.32) \quad (10)$$

where $2.32 = \text{ASC}_{\text{BASIC}}$. Parameters which were invariant for flow approaching the vehicle from either the bow or aft end (*TSHT*, *SSL*, *XLB*, and *ER*) were not changed. For example

$$(\Delta C_{D_{XLB}})_{135°-180°}(\beta) = (\Delta C_{D_{XLB}})_{45°-0°}(\beta) \quad (11)$$

There remains the problem of how to predict C_D between 45° and 135°. It was determined empirically that

$$C_D(\beta = 90°) = [C_D(\beta = 0°) + C_D(\beta = 180°)](SA/FA)/2 \quad (12)$$

where SA = projected area of the vehicle under consideration at $\beta = 90°$ (i.e., the side area), and FA = projected frontal area at $\beta = 0°$, 180°.

Next, the total C_D's for the obtained points are found from Eq. (1), then an eighth-order curve fit is made to them (i.e., $\beta = 0°$–45°, $\beta = 90°$, and $\beta = 135°$–180°), and the variation of C_D from $\beta = 45$–135° obtained from this curve fit.

The methods used for the side force coefficient (C_Y) and yawing moment coefficient (C_N) components are exactly the same as those used for drag. Table 1 presents the order of variations with geometry parameters for C_Y and C_N. It was decided to predict yawing moment coefficient independently of the drag and side force. From experience it has been found that by using drag and side force and predicting center of pressure and multiplying the appropriate forces by moment arms, large errors are frequently introduced in the resulting yawing moment due to devastating multiplicative errors. There was one exception to this decision. The yawing moment at $\beta = 90°$ was found as follows:

$$C_N(\beta = 90°) = [C_D(\beta = 90°) \times (XCP - XCG]/1 \quad (13)$$

where *XCG* is the desired moment reference point or center of gravity measured from aft end of the vehicle, 1 is the vehicle length, and *XCP* is the center of pressure measured from the aft end at $\beta = 90°$; *XCP* was approximated by the centroid of the side projected area *SA*. However, small errors in *XCP* introduce large errors in the predicted C_N, and great care and some insight into the effects of fore and aft geometrical asymmetries must be used to correctly determine *XCP*.

The following equation was used in the prediction of the side force at $\beta = 90°$:

$$C_Y(\beta = 90°) = [C_Y(\beta = 45°) + C_Y(\beta = 135°)]/2 \cdot |RC_Y| \quad (14)$$

where

$$|RC_Y| \equiv \left|\frac{C_Y(\beta = 135°)}{C_Y(\beta = 45°)}\right| \quad \text{or} \quad \left|\frac{C_Y(\beta = 45°)}{C_Y(\beta = 135°)}\right|$$

whichever has a magnitude less than 1.0.

The total C_Y and C_N are then found from Eq. (1).

Cushion Effects, and Velocity Effects

It should be mentioned that the changes in aerodynamic coefficients due to geometry changes have been treated only linearly, per Eq. (1), in this paper; i.e., cross-coupling effects, whereby a charge in one geometry parameter may affect the

variations in C_D, C_Y, C_N due to changes in another geometry parameter, have been neglected. Comparisons of the predicted coefficients with available wind-tunnel data on several configurations have indicated that either the cross-coupling effects are small or they are fortuitously accounted for in the presented linear analysis. However, possible cross-coupling effects are being investigated more thoroughly by the authors.

Another problem not covered in the foregoing analysis is that of the effects of cushion efflux and inlet influx on the external aerodynamics of the vehicle. This important problem needs detailed investigation, and work is progressing in this area. Walker[4] indicates that the cushion efflux effects can be divided into several distinct flow regimes depending on the relative magnitude of cushion pressure and freestream dynamic pressure q (Fig. 9). In the Arctic ACV program, interest is primarily in q's of 50 psf or less and cushion pressures greater than 80 psf. Therefore, there will be no interest in the supercritical regime.

Andrews[3] has conducted valuable experimental investigations. For blowing only (i.e., cushion efflux but no inlet influx) his results indicate a decrease in drag in beamwind conditions but little effect of cushion efflux on side force at yaw angles near 0 and 180°. However, increasing the cushion efflux increases the yaw angle for zero side force. Yawing moment appears to be only slightly affected by cushion efflux. These effects are illustrated in Fig. 10.

Though these blowing-only results are instructive, the problem of interest will be that of simultaneous blowing and inlet influx. Andrews' data for a configuration with the inlets on the rear of the craft show that the combined effects of influx and efflux are much more complicated than those for efflux alone, particularly in the case of drag. The yawing moment coefficient C_N peaks at higher values near $\beta = 40°$ and 130° than in the no internal flow case, and side force magnitude decreases if the wind is from the fore part of the craft and increases if it is from the aft, as shown in Fig. 11.

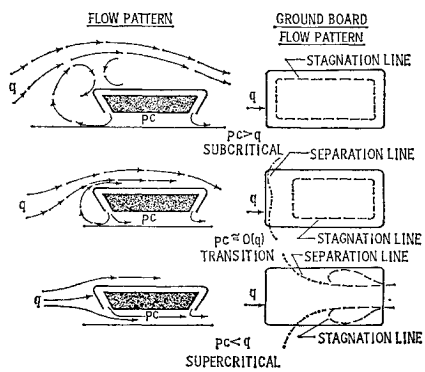

Fig. 9 Flow regimes for cushion efflux for thick jets or plenum type craft.

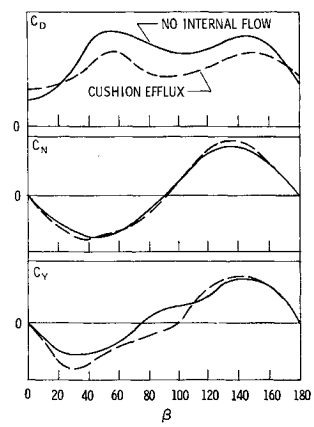

Fig. 10 Effects of cushion efflux only on external aerodynamics.

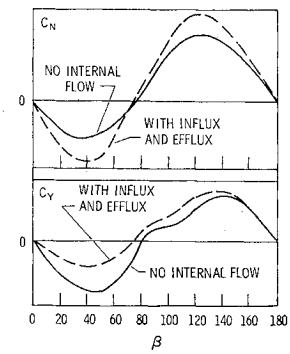

Fig. 11 Effects of influx and efflux on external aerodynamics.

Because Andrews presents influx-efflux data for only one configuration, and these influx-efflux effects may depend on configuration, no attempt was made to include them in the present prediction method for general configurations. However, the authors hope to run influx-efflux tests on several other configurations and to incorporate the results in the prediction, in much the same manner as the vehicle geometrical effects were handled. That is

$$C_{D,Y,N\ \text{INFLUX EFFLUX}} = C_{D,Y,N\ \text{WITHOUT INFLUX EFFLUX}} + \Delta C_{D,Y,N\ \text{DUE TO INFLUX EFFLUX}}$$

where

$$\Delta C_{D,Y,N\ \text{DUE TO INFLUX EFFLUX}} = \text{function of (cushion pressure, } V, \beta, \text{ configuration, inlet geometry)}$$

Since it appears from Walker's studies that the effects of varying the freestream velocity are very much interconnected with the cushion pressure, analysis of velocity effects will await the investigation of cushion effects. The present analysis has been programed for V between 117 and 190 fps, and the aerodynamic *coefficients* appear practically invariant between these speeds.

Results

Figure 12 shows the four ACV configurations for which the predicted aerodynamic curves have been compared to experimental data, without influx and efflux. The data for configurations 1 and 2 were obtained at NSRDC, and those for configurations 3 and 4 were obtained by Andrews.[3] Unfortunately, the experimental data for configurations 1 and 2, Fig. 13, are limited to $0 \leqslant \beta \leqslant 45°$.

It is apparent from these comparisons that drag may be underpredicted for certain configurations at $\beta > 20°$. However, for gross range prediction, the craft most probably operates a large percentage of the time at $\beta \cong 0$ and this underprediction is not serious. Also, for maneuvers at $0° \leqslant \beta \leqslant 60°$, the yawing moment and side force, which are predicted more accurately, are more imporant. The yawing

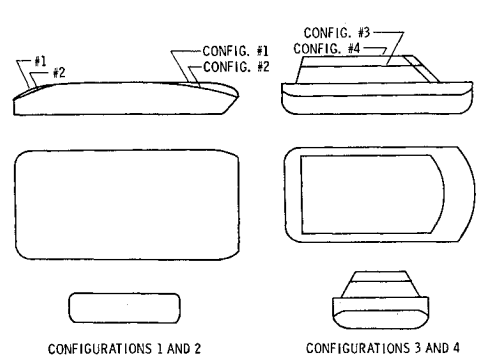

Fig. 12 Configurations used to compare prediction and experiment.

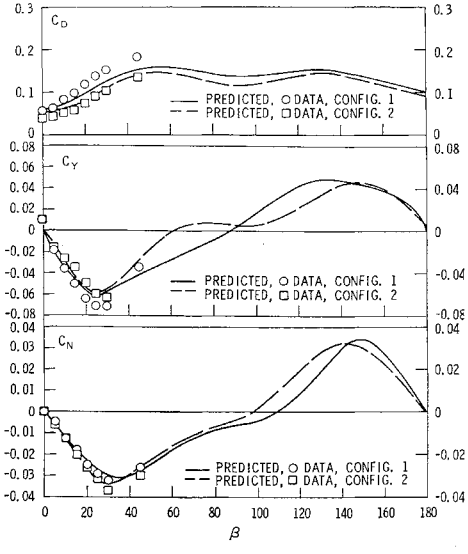

Fig. 13 Comparison of prediction and data for configurations 1 and 2.

moment inaccuracies for $60° \leqslant \beta \leqslant 150°$ in Fig. 14 are primarily caused by inadequate estimation of the center of pressure at $\beta = 90°$ using the centroid of projected area method; the inaccuracy shown is due to an error of approximately 0.5% in XCP/l for configurations 3 and 4.

The aerodynamic prediction has been computerized and mated with a three-degree-of-freedom (lateral, longitudinal, and yaw motions) vehicle dynamics program developed at NSRDC. The digital vehicle dynamics program uses a step-by-step integration of the equations of motion. At any particular time step it requires the vehicle aerodynamic forces as inputs. The vehicle dynamics program knows the vehicle velocity and attitude and geometry at any time step, goes to the present aerodynamics program to compute the aerodynamic forces, and returns to integrate to the next time step. Thus, the present program allows prediction of craft motions, and definition of optimum ACV shapes with respect to the external aerodynamic force field. The design engineer can use the program to obtain preliminary definitions of low-drag configurations, which result in increased range, and high-side-force and yawing-moment configurations resulting in high maneuverability.

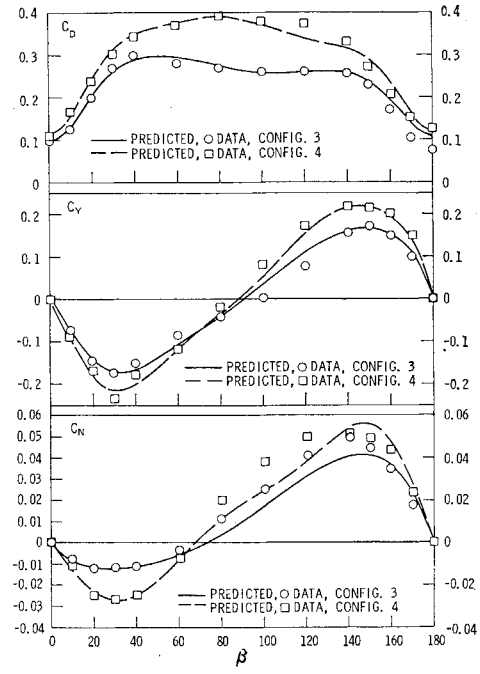

Fig. 14 Comparison of prediction and data configurations 3 and 4.

References

[1] Zeitfuss, W., Private Communication on Wind Tunnel Tests of Basic Geometry Variations, Naval Ship Research and Development Center, Washington, D.C.

[2] Wilson, F. W., "A Parametric Investigation of Captured Air Bubble Vehicle Aerodynamic Drag and Other Characteristics," Rept. 3657, April 1971, Naval Ship Research and Development Center, Washington, D.C.

[3] Andrews, E. J., "The External Aerodynamics of Hovercraft," *von Kármán Institute for Fluid Dynamics, Lecture Series 33, Aerodynamics of Air Cushion Vehicles*, Rhode-Saint-Genese, Belgium, Feb. 1971.

[4] Walker, N. K., "Some Notes on the Lift and Drag of Ground Effect Machines," *Proceedings of the National Meeting on Hydrofoils and Air Cushion Vehicles*, Institute of the Aerospace Sciences, Washington, D.C., Sept. 1962, pp. 65–80.